



ELSEVIER

Characteristics of superplasticity domain in the processing map for hot working of as-cast Mg–11.5Li–1.5Al alloy

O. Sivakesavam ^{a,*}, Y.V.R.K. Prasad ^b

^a Defence Metallurgical Research Laboratory, Research and Development Organisation, Government of India, PO: Kanchanbagh, Hyderabad 500058, Andhra Pradesh, India

^b Department of Metallurgy, Indian Institute of Science, Bangalore 560012, Karnataka, India

Received 25 August 2000; received in revised form 26 March 2001

Abstract

Processing map for hot working of as-cast Mg–11.5Li–1.5Al alloy has been developed in the temperature range 200–450°C and strain rate range 0.001–100 s⁻¹. The map exhibited a single domain with a peak efficiency of 65% occurring at 400°C and 0.001 s⁻¹. Under these conditions, the material exhibited abnormal elongation. On the basis of the elongation, the grain structure, the apparent activation energy for hot deformation (95 kJ mole⁻¹) and the peak efficiency of power dissipation (65% corresponding to a strain rate sensitivity of about 0.5), the domain is interpreted to represent superplasticity. At strain rates higher than about 10 s⁻¹, the material exhibits microstructural instability, while at temperatures of 450°C and a strain rate of 0.001 s⁻¹, grain boundary cracking is observed. © 2002 Elsevier Science B.V. All rights reserved.

Keywords: Mg–Li alloys; Superplasticity; Hot working; Processing maps

1. Introduction

The occurrence of superplasticity in magnesium alloys has been studied for over three decades and the results have been reviewed recently [1]. Most of the studies have been on Mg–Zn–Zr or Mg–Al–Zn alloys with fine grained microstructures. In the previous decade, the study of superplasticity in low density Mg–Li system has assumed importance in aerospace and automobile applications in view of its high specific stiffness. Mg–Li alloys with lithium content higher than about 10.3 wt.% have base centered cubic (bcc) structure (β -phase). The addition of aluminum stabilizes its properties and makes the alloy suitable for engineering applications [2]. At elevated temperatures, Mg–Li alloys exhibit superplasticity [3–5] in the temperature range 150–250°C and the activation energy for superplastic flow is equal to that for lattice diffusion in the β -phase [3]. The aim of the present investigation

is to study the hot deformation behavior of Mg–11.5Li–1.5Al alloy using processing maps with particular reference to the domain of superplasticity. The processing maps are developed on the basis of Dynamic Materials Model [6], which is recently reviewed by Prasad and Seshacharyulu [7]. In this model, the work-piece is considered to be a dissipator of power and at any instant the total power dissipated consists of two complementary parts, G content representing dissipation through a temperature rise and J co-content representing the dissipation through metallurgical processes. The factor that partitions power between G and J is the strain rate sensitivity (m) of flow stress. The strain rate sensitivity is the inverse of the stress exponent (n) in the standard kinetic rate equation describing the hot deformation. The J co-content is given by [6]:

$$J = \int_0^{\bar{\sigma}} \dot{\varepsilon} d\bar{\sigma} = \frac{\bar{\sigma} \bar{\varepsilon} m}{m + 1} \quad (1)$$

where $\bar{\sigma}$ is the flow stress and $\bar{\varepsilon}$ is the strain rate. For an ideal linear dissipator, $m = 1$ and $J = J_{\max} = \bar{\sigma} \bar{\varepsilon} / 2$. The efficiency of power dissipation of a non-linear dissipator may be expressed as a dimensionless parameter:

* Corresponding author. Tel.: +91-40-4345865; fax: +91-40-4341439.

E-mail address: prasad@metalrg.iisc.ernet.in (Y.V.R.K. Prasad).

$$\eta = \frac{J}{J_{\max}} = \frac{2m}{m+1} \quad (2)$$

The variation of η which is usually expressed as percent, with temperature and strain rate represents the power dissipation characteristics occurring through microstructural changes in the workpiece material and constitutes a power dissipation map. This map exhibits different domains, which may be correlated with specific microstructural processes.

The dynamic materials model has as its basis the extremum principles of irreversible thermodynamics as applied to large plastic flow described by Ziegler [8]. Kumar [9] and Prasad [10] developed a continuum criterion combining these principles with those of separability of power dissipation and have shown that flow instability will occur during hot deformation if:

$$\xi(\dot{\varepsilon}) = \frac{\partial \ln[m/(m+1)]}{\partial \ln \dot{\varepsilon}} + m \leq 0 \quad (3)$$

The variation of the instability parameter $\xi(\dot{\varepsilon})$ with temperature and strain rate constitutes an instability map, which may be superimposed on the power dissipation map for obtaining an instability map. This methodology has been used to optimize hot workability of a variety of materials [11] including as-cast magnesium [12].

2. Experimental

Mg–Li–Al alloys were prepared by mixing molten magnesium and aluminum in a mild steel crucible at about 750°C and pouring over molten lithium separately melted in a stainless steel crucible and kept at around 300°C. The melt was chill cast in a cast iron mould. The average grain diameter of the as-cast ingot was about 470 μm. Cylindrical specimens of 10 mm diameter and 15 mm height were machined from the ingot and used for compression testing. The tempera-

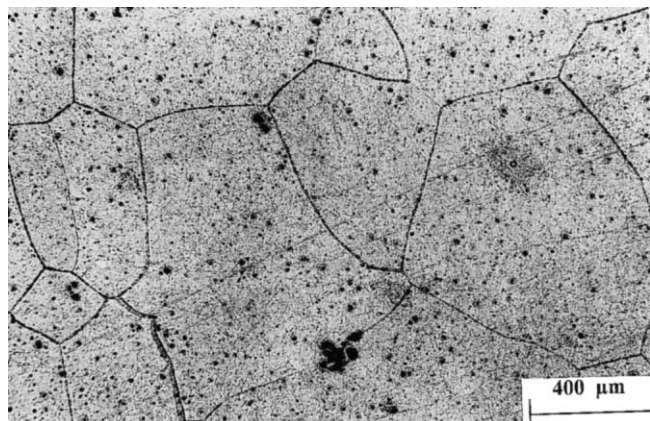


Fig. 1. Initial microstructure of as-cast Mg–11.5Li–1.5Al alloy showing β-solid solution.

ture of the specimen was monitored with the aid of a chromel/alumel thermocouple embedded in a 0.8 mm diameter hole machined at half the height of the specimen. This thermocouple was also used for measuring the adiabatic temperature rise in the specimen during deformation. A computer controlled servohydraulic testing machine (DARTEC, UK) was used for hot compression tests.

The machine was equipped with an exponentially decaying cross head speed, enabling constant true strain rates in the range 0.001–100 s⁻¹ to be imposed on the specimen. Isothermal tests were conducted by surrounding the specimen, platens and pushrods with a resistance furnace with a control of temperature within ± 2°C. The adiabatic temperature rise was also measured on the specimen using the embedded thermocouple and a Nicolet transient recorder.

The tests were conducted over a temperature range of 200–450°C at intervals of 50°C and in the strain rate range of 0.001–100 s⁻¹. In each test, the specimen was compressed to about half its original height and the load–displacement data were recorded.

The procedure for obtaining the power dissipation maps was as follows. The load–displacement curves obtained in compression at constant temperature and true strain rate were converted into true stress and true plastic strain curves using standard equations. The flow stress data as a function of temperature and strain rate were obtained from these curves and used to construct the power dissipation maps. The log(flow stress) versus log(strain rate) data were fitted using a cubic spline and the strain rate sensitivity (m) was calculated as a function of strain rate. This was repeated for various temperatures investigated. The efficiency of power dissipation through microstructural changes [$\eta = 2m/(m+1)$] was then calculated as a function of temperature and strain rate and plotted as an iso-efficiency map. The values of $\xi(\dot{\varepsilon})$ given by Eq. (3) were also evaluated and plotted as a function of temperature and strain rate to give an instability map.

The deformed specimens were water quenched and some selected deformed specimens were sectioned parallel to the compression axis and prepared for metallographic examination. The specimens were etched with 2% nital. Cylindrical specimens were also machined for tensile testing at a strain rate of 0.001 s⁻¹ and these had a gauge length of 25 mm and a gauge diameter of 4 mm.

3. Results

The initial microstructure of the alloy is shown in Fig. 1 which is a single phase structure. Typical true stress–true strain curves recorded at 400°C at different strain rates are shown in Fig. 2. The curves recorded at

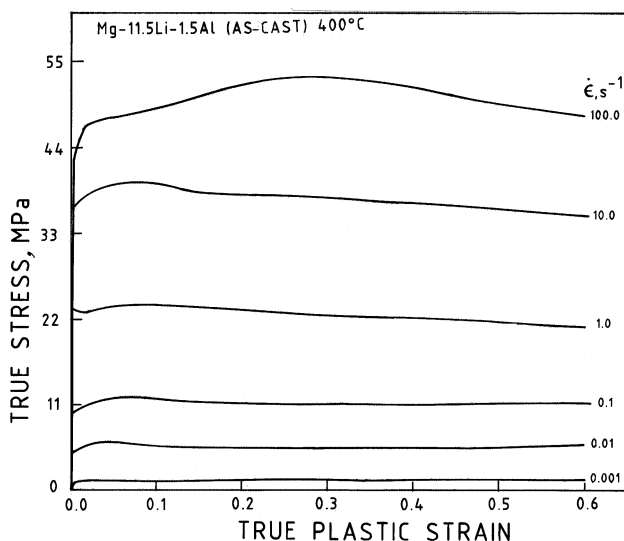


Fig. 2. True stress–true strain curves on as-cast Mg–11.5Li–1.5Al alloy at 400°C and different strain rates.

other temperatures are essentially similar to those shown in Fig. 2. Up to a strain rate of 1.0 s^{-1} , the

stress–strain curves exhibited steady state behavior while at strain rates higher than 10 s^{-1} the curves exhibited uneven shapes. The flow stress data obtained as a function of strain rate and temperature are given in Table 1. These data are corrected for the adiabatic temperature rise measured on the specimens during deformation. The correction was done using linear interpolation [7] of log(flow stress) versus inverse of absolute temperature plots. The correction was found to be important at strain rates higher than 1.0 s^{-1} since at lower strain rates, the adiabatic temperature rise was not significant enough to warrant a correction.

The power dissipation map obtained at a strain of 0.4 is shown in Fig. 3. The maps obtained at other strains are similar indicating that strain does not have a significant effect. The map exhibits a single domain with a peak efficiency of about 65% occurring at 400°C and 0.001 s^{-1} . The instability map developed on the basis of the continuum criterion given by Eq. (3) is shown in Fig. 4 for a strain of 0.4. The material is likely to flow in an unstable fashion in the regime above the contour ' H ', i.e. where $\xi(\dot{\epsilon})$ is negative. The microstructural manifestation of the instability is discussed later.

Table 1
Flow stress values for as-cast Mg–11.5Li–1.5Al alloy at various strains, strain rates and temperatures^a

| Strain | Strain rate (s^{-1}) | Flow stress (MPa) at temperature (0°C) of | | | | | |
|--------|--------------------------|---|-------|------|------|------|------|
| | | 200 | 250 | 300 | 350 | 400 | 450 |
| 0.1 | 0.001 | 28.3 | 17.1 | 7.0 | 4.0 | 1.2 | 0.9 |
| | 0.010 | 40.7 | 29.6 | 16.2 | 9.3 | 5.5 | 2.5 |
| | 0.100 | 56.9 | 46.6 | 32.5 | 19.2 | 11.5 | 7.0 |
| | 1.000 | 82.0 | 67.0 | 54.0 | 38.0 | 25.0 | 17.0 |
| | 10.000 | 123.0 | 85.0 | 72.0 | 57.0 | 41.0 | 29.0 |
| | 100.000 | 126.0 | 101.0 | 82.0 | 64.0 | 51.0 | 38.0 |
| 0.2 | 0.001 | 26.6 | 15.7 | 6.7 | 3.9 | 1.5 | 0.8 |
| | 0.010 | 39.9 | 28.4 | 16.3 | 9.1 | 5.6 | 2.9 |
| | 0.100 | 57.0 | 45.8 | 32.3 | 18.8 | 11.3 | 7.1 |
| | 1.000 | 81.0 | 66.0 | 53.0 | 38.0 | 24.0 | 16.0 |
| | 10.000 | 117.0 | 83.0 | 71.0 | 56.0 | 40.0 | 28.0 |
| | 100.000 | 127.0 | 104.0 | 85.0 | 66.0 | 54.0 | 39.0 |
| 0.3 | 0.001 | 26.6 | 15.1 | 6.7 | 3.9 | 1.3 | 1.0 |
| | 0.010 | 39.4 | 28.1 | 15.8 | 9.1 | 5.6 | 2.9 |
| | 0.100 | 56.5 | 45.6 | 32.0 | 18.6 | 11.1 | 7.0 |
| | 1.000 | 79.0 | 66.0 | 52.0 | 37.0 | 24.0 | 16.0 |
| | 10.000 | 110.0 | 81.0 | 71.0 | 55.0 | 40.0 | 28.0 |
| | 100.000 | 125.0 | 107.0 | 87.0 | 68.0 | 55.0 | 40.0 |
| 0.4 | 0.001 | 26.5 | 14.6 | 6.9 | 4.0 | 1.4 | 1.1 |
| | 0.010 | 39.7 | 27.9 | 15.9 | 9.4 | 5.6 | 2.9 |
| | 0.100 | 55.4 | 45.5 | 31.4 | 18.6 | 11.3 | 7.0 |
| | 1.000 | 77.0 | 64.0 | 51.0 | 38.0 | 23.0 | 16.0 |
| | 10.000 | 108.0 | 80.0 | 70.0 | 55.0 | 39.0 | 28.0 |
| | 100.000 | 126.0 | 103.0 | 84.0 | 66.0 | 53.0 | 39.0 |
| 0.5 | 0.001 | 27.1 | 14.8 | 7.1 | 3.9 | 1.5 | 1.3 |
| | 0.010 | 39.2 | 28.0 | 15.7 | 9.9 | 5.8 | 2.8 |
| | 0.100 | 56.5 | 45.4 | 30.9 | 18.5 | 11.1 | 6.7 |
| | 1.000 | 74.0 | 65.0 | 51.0 | 38.0 | 23.0 | 15.0 |
| | 10.000 | 107.0 | 78.0 | 68.0 | 53.0 | 39.0 | 27.0 |
| | 100.000 | 119.0 | 98.0 | 81.0 | 65.0 | 51.0 | 37.0 |

^a Data corrected for adiabatic temperature increase.

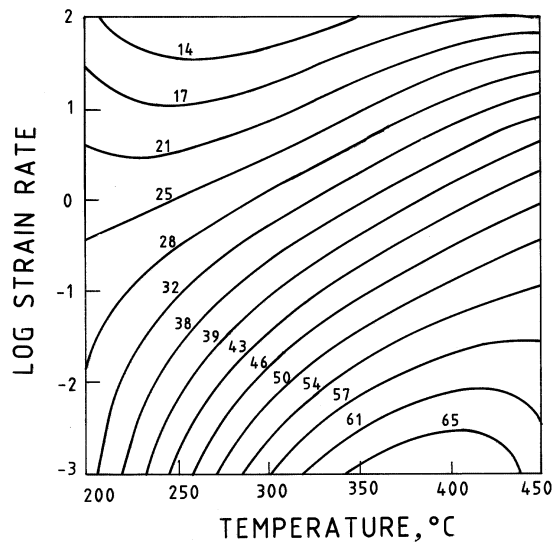


Fig. 3. Power dissipation map on as-cast Mg–11.5Li–1.5Al alloy at a strain of 0.4. The contours represent iso-efficiency expressed as percent.

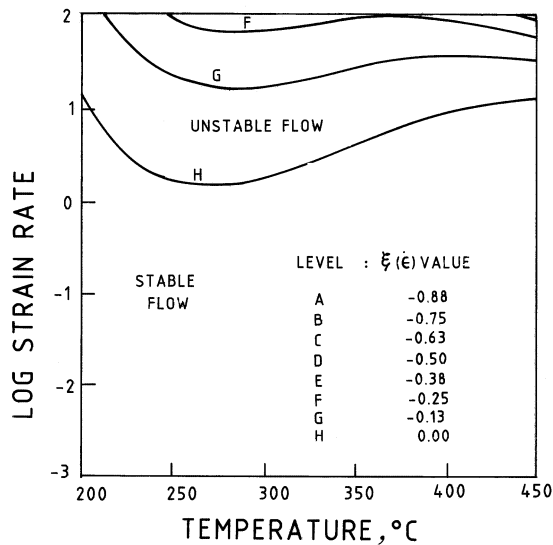


Fig. 4. Instability map obtained on as-cast Mg–11.5Li–1.5Al alloy at a strain of 0.4. The material is unstable above the region marked by contour 'H' where $\xi(\dot{\epsilon})$ is negative.

4. Discussion

4.1. Domain of superplasticity

As per Raj maps [13] the domain occurring at higher temperatures ($0.75 T_m$) and lower strain rates ($< 0.001 \text{ s}^{-1}$) represents the process of grain boundary sliding. The stress concentrations occurring at the grain boundary triple junctions, if not relieved by accommodation processes, will result in wedge cracking. However, in the case of superplastic deformation, the triple junction stresses are relieved by diffusion accommodated flow [14] and therefore extensive ductilities are

achieved. Thus, the high temperature–low strain rate regime of Raj maps represents superplasticity under conditions of diffusion accommodated flow. In view of these correlations, the domain occurring at 400°C and 0.001 s^{-1} in the power dissipation map (Fig. 3) of as-cast Mg–Li–Al alloy may be interpreted to represent superplastic deformation. The efficiency of power dissipation for superplasticity is much higher than 50% and is ideally at 65%, which corresponds to a strain rate sensitivity of 0.5. This interpretation is confirmed by the following observations.

1. The tensile elongations measured on the specimens at different temperatures across the domain are shown in Fig. 5a. The values are large and are consistent with those reported in the literature [1,3]. Also the variations of tensile ductility and the efficiency of power dissipation are similar and the temperature and strain rate for the efficiency peak result in the highest ductility.
2. The grain size variation with temperature is very small (Fig. 5b) and if at all any change is noticed, it is a minor grain growth. Further the ‘orientation’ of the grain boundaries is measured in terms of the angle between the trace of the grain boundary on the

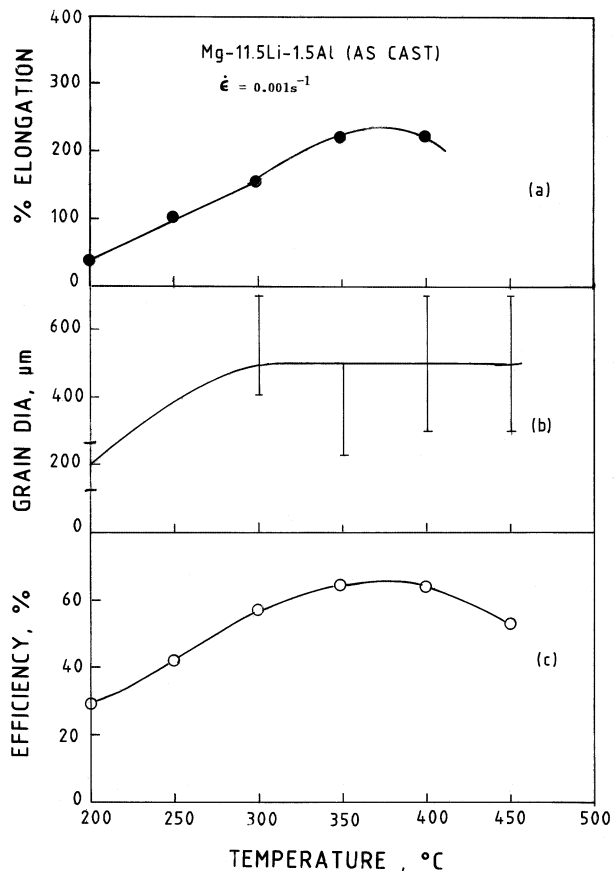


Fig. 5. Variation of (a) tensile ductility, (b) grain size and (c) efficiency with temperature for as-cast Mg–11.5Li–1.5Al alloy in the superplastic domain at the strain rate of 0.001 s^{-1} .

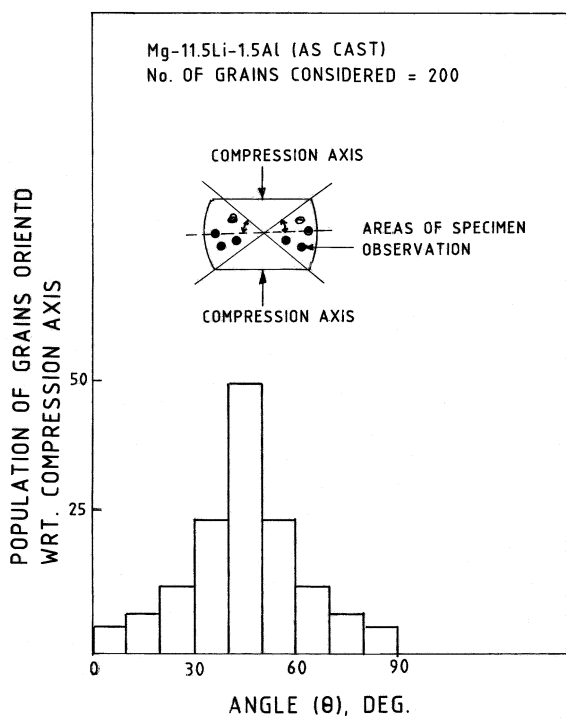


Fig. 6. Orientation of grain boundary traces with respect to the compression axis of the specimen deformed at 400°C and 0.001 s^{-1} .

micrograph with respect to the compression axis. These values corresponding to the specimen deformed at 400°C and 0.001 s^{-1} (peak efficiency conditions for superplasticity domain) are shown in Fig. 6 in the form of a bar graph. A high population of these boundaries is oriented between 40 and 50° indicating that the shear stress resolved on these boundaries has caused sliding. Typical microstructures of the specimens deformed under conditions of superplasticity are shown in Fig. 7a and b, which correspond to $200^\circ\text{C}/0.001\text{ s}^{-1}$ and $400^\circ\text{C}/0.001\text{ s}^{-1}$, respectively. The shape of the grain boundaries is equiaxed in these microstructures, which is also a hallmark of superplasticity. Similar equiaxed microstructures are also observed under other deformation conditions within the domain as seen in the microstructures of specimens deformed at 400°C and at 0.01, 0.1 and 1.0 s^{-1} (Fig. 8a–c).

- As the domain extends over a wide temperature and strain rate range, the kinetic analysis may be applied to evaluate the apparent activation energy for hot deformation in this alloy. The kinetic rate equation for hot deformation is given by:

$$\dot{\varepsilon} = A\sigma^n \exp\left[\frac{-Q}{RT}\right] \quad (4)$$

where A is the constant, n the stress exponent, Q the activation energy, R the gas constant and T is

the temperature in Kelvin. On the basis of $\log(\dot{\varepsilon})$ versus $\log(T)$ plots, the value of n is estimated to be about 3.0. The plot of $[n \log(\dot{\varepsilon})]$ vs. $(1/T)$ is shown in Fig. 9 from the slope of which the apparent activation energy is estimated to be about 95 kJ mole $^{-1}$. This value is somewhat smaller than the activation energy for self-diffusion in Mg (134 kJ mole $^{-1}$). The data on the activation energy for diffusion of Li in Mg are not available but in view of the smaller atomic radius of Li (0.151 nm) and the open bcc structure of the β -phase, it is likely that the activation energy for diffusion is smaller than that for self-diffusion in Mg. The measured value of the apparent activation energy is suggestive of easy diffusion and the lower value is responsible for a faster diffusion accommodated flow causing superplasticity in this material.

It is interesting to note that Mg–Li–Al alloy does not exhibit dynamic recrystallization (DRX) domain even in this wide temperature–strain rate range. This may be due to the high rate of diffusion, which will

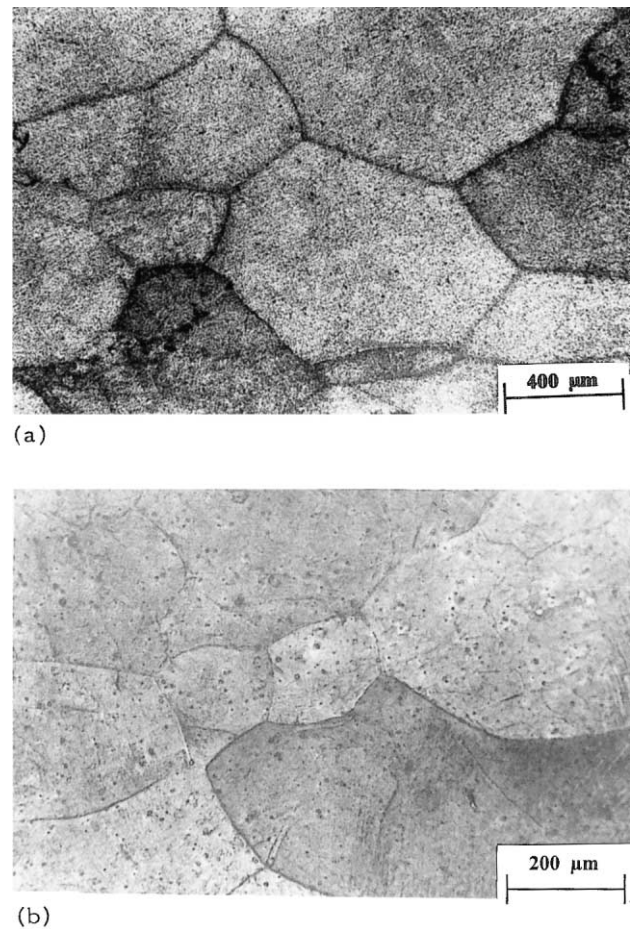
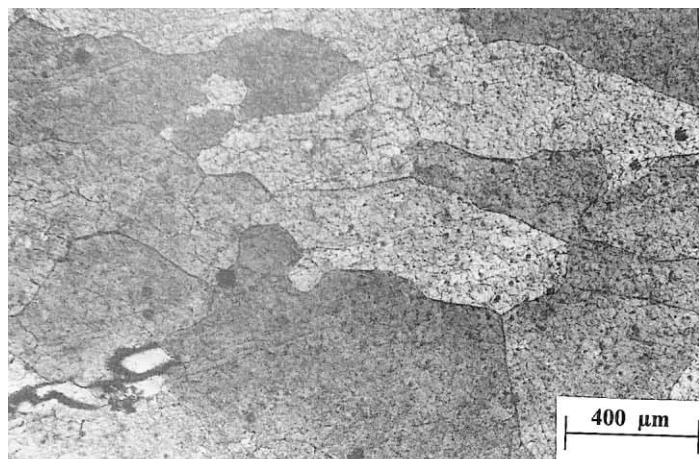
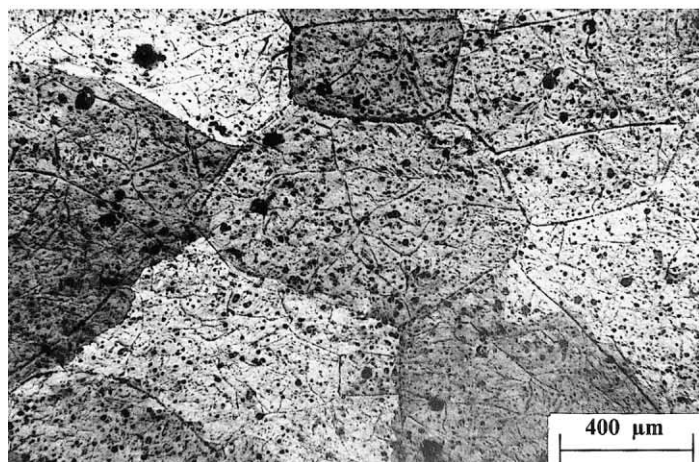


Fig. 7. Microstructures of specimens deformed under conditions of superplasticity (a) $200^\circ\text{C}/0.001\text{ s}^{-1}$ and (b) $400^\circ\text{C}/0.001\text{ s}^{-1}$.



(a)



(b)

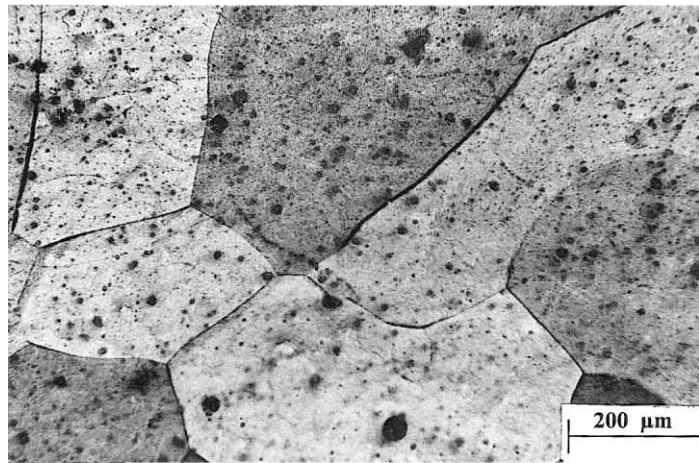


Fig. 8. Microstructures of specimens showing superplasticity over extended region of strain rates, (a) 400°C/0.01 s⁻¹ (b) 400°C/0.1 s⁻¹ and (c) 400°C/1 s⁻¹.

not permit the formation of DRX nuclei because of annihilation of dislocations by faster recovery processes.

4.2. Intercrystalline cracking

At higher temperature than the optimum superplastic range, the material exhibits grain growth and intercrystalline fracture after deformation. A typical micrograph recorded on specimen deformed at 450°C and 0.001 s⁻¹ and at 100 s⁻¹ are shown in Fig. 10a and b, respectively. Both these micrographs exhibit grain boundary cracking. At this temperature, grain boundary cracking is also exhibited by the specimens deformed at all other intermediate strain rates.

4.3. Flow instabilities

As per the instability criterion (Eq. (3)), the material is expected to show some unusual features like flow localization at strain rates higher than 10 s⁻¹. Microstructures of the specimen deformed at 200°C/10 s⁻¹ and 200°C/100 s⁻¹ exhibited flow localization as shown in Fig. 11a and b, respectively. Strain rates higher than 10 s⁻¹ may be avoided in processing this material.

4.4. Comparison with other magnesium alloys

Superplasticity has been reported on other magnesium alloy systems like Mg-Al-Zn (AZ31) and Mg-Zn-Zr (ZK60), although the required grain sizes in these systems are very fine (less than 15 μm) [15]. Very fine grain sizes of the order of 2 μm give high strain rate superplasticity in these alloys [16]. In Mg-Li alloy system, superplasticity is observed at homologous tem-

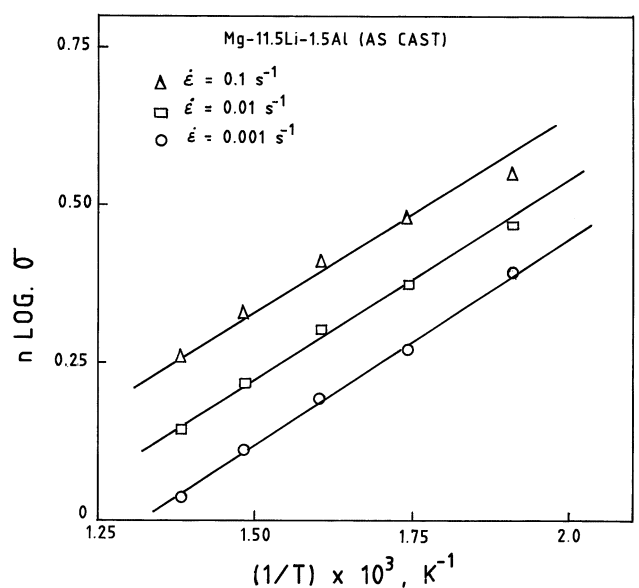
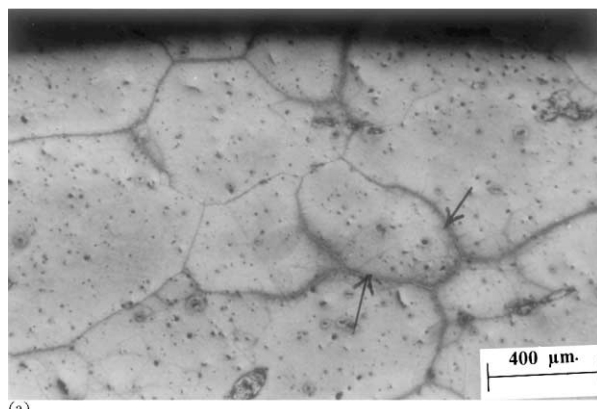
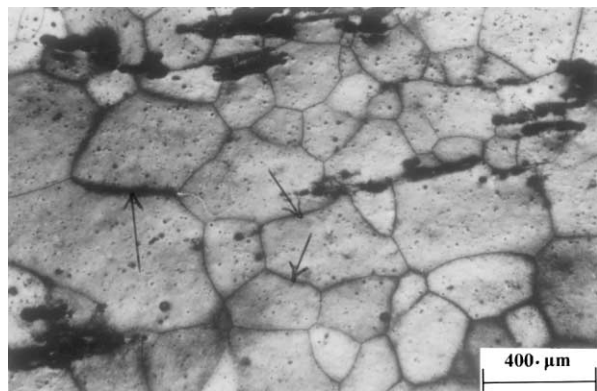


Fig. 9. Variation of $[n \log(\sigma)]$ vs. $(1/T)$ for hot deformation of as-cast Mg-11.5Li-1.5Al alloy giving an apparent activation energy of 95 kJ mole⁻¹.



(a)



(b)

Fig. 10. Microstructures of specimens showing grain growth and intercrystalline(grain boundary) fracture after deformation above optimum superplastic temperature. (a) Specimen deformed at $450^{\circ}\text{C}/0.001 \text{ s}^{-1}$ and (b) $450^{\circ}\text{C}/100 \text{ s}^{-1}$ (fracture paths of grain boundaries shown with arrows).

peratures as low as 0.4–0.5 when the grain size is made very fine using thermomechanical treatments [3]. In as-cast and rapidly solidified magnesium alloy AZ91, superplastic properties have been reported [17] and the elongations in the latter case were large due to fine grain size. However, while most of the superplastic deformation studies have been on fine grained wrought alloys, the present observation of superplasticity in as-cast Mg–Li–Al alloy is on a large grained material (about $450 \mu\text{m}$) and hence is a very significant result. Moreover, such superplasticity is not associated with the formation of fine grains or subgrains during deformation but by a process involving large scale diffusional processes in the system. The application of such a process offers immense possibilities of using the as-cast alloy strip or part for several applications such as automobiles with considerable cost savings since the steps of thermomechanical processing can be avoided.

5. Conclusions

(1) A domain of superplasticity occurs in the processing map for large grained as-cast Mg–11.5Li–1.5Al

alloy with a peak efficiency of 65% occurring at 400°C and a strain rate of 0.001 s^{-1} .

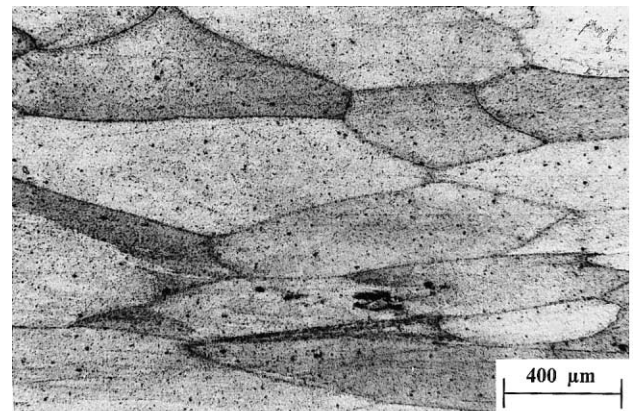
(2) The apparent activation energy for hot deformation in the superplasticity domain is 95 kJ mole^{-1} which is lower than that for self-diffusion in Mg (134 kJ mole^{-1}).

(3) At strain rates higher than 10 s^{-1} , the material exhibits flow instability, which manifests as flow localization.

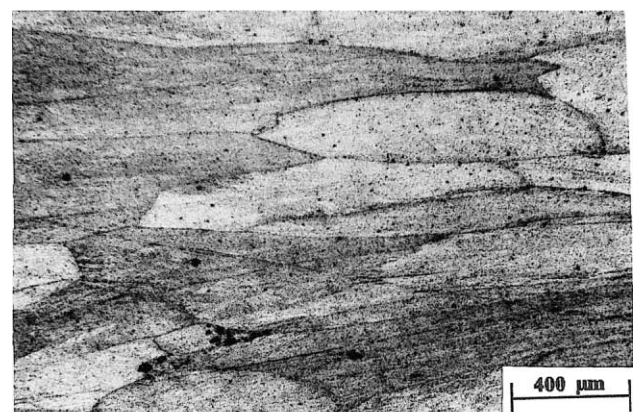
(4) At a temperature of 450°C , which is higher than the optimum temperature for superplastic deformation, the material exhibits intercrystalline cracking.

Acknowledgements

One of the authors (O. Sivakesavam) is thankful to Dr D. Banerjee, Director of Defence Metallurgical Research Laboratory, Hyderabad, India for permission to publish this paper.



(a)



(b)

Fig. 11. Instability microstructures due to flow localization in the instability domain at higher strain rates, (a) $200^{\circ}\text{C}/10 \text{ s}^{-1}$; (b) $200^{\circ}\text{C}/100 \text{ s}^{-1}$.

References

- [1] T.G. Nieh, J. Wadsworth, O.D. Sherby, Superplasticity in Metals and Ceramics, Cambridge University Press, Cambridge, UK, 1997, p. 69.
- [2] J.C. McDonald, Trans. ASM 61 (1968) 505.
- [3] P. Metenier, G. Gonzalez-Doncel, O.A. Ruano, J. Wolfenstein, O.D. Sherby, Mater. Sci. Eng. A125 (1990) 195.
- [4] O.A. Kaibyshev, Superplasticity of Alloys, Intermetallides and Ceramics, Springer, Berlin, 1992, p. 316.
- [5] E.I. Emeley, Principles of Magnesium Technology, Pergamon Press, London, 1966.
- [6] Y.V.R.K. Prasad, H.L. Gegel, S.M. Doraivelu, J.C. Malas, J.T. Morgan, K.A. Lark, D.R. Barker, Metall. Trans. A15 (1984) 1883.
- [7] Y.V.R.K. Prasad, T. Seshacharyulu, Int. Mater. Rev. 43 (1998) 243.
- [8] H. Ziegler, in: I.N. Sneddon, R. Hill (Eds.), Progress in Solid Mechanics, vol. 4, North Holland, Amsterdam, 1963, p. 93.
- [9] A.K.S. Kalyan Kumar, Criteria for Predicting Metallurgical Instabilities in Processing, M.Sc. (Engineering) thesis, Indian Institute of Science, Bangalore, India, 1987.
- [10] Y.V.R.K. Prasad, Indian J. Technol. 28 (1990) 435.
- [11] Y.V.R.K. Prasad, S. Sasidhara, Hot Working Guide: A Compendium of Processing Maps, ASM International, Materials Park, OH, 1997.
- [12] O. Sivakesavam, I.S. Rao, Y.V.R.K. Prasad, Mater. Sci. Technol. 9 (1993) 805.
- [13] R. Raj, Metall. Trans. A12 (1981) 1089.
- [14] M.F. Ashby, R.A. Verrall, Acta Metall. 21 (1973) 149.
- [15] A. Bussiba, A. Ben Artzy, A. Shtechman, S. Ifergan, M. Kupiec, Mater. Sci. Eng. A302 (2001) 56.
- [16] A. Mukai, H. Watanabe, K. Higashi, Mater. Sci. Technol. 16 (2000) 1314.
- [17] J.K. Solberg, J. Torklep, O. Bauger, H. Gjestland, Mater. Sci. Eng. A134 (1991) 1201.